

DETECTION OF WEAK GRAVITATIONAL LENSING MAGNIFICATION FROM GALAXY-QSO CROSS-CORRELATION IN THE SDSS

ENRIQUE GAZTAÑAGA

Institut d'Estudis Espacials de Catalunya, IEEC/CSIC, Gran Capitá 2-4, 08034 Barcelona, Spain

Draft version December 2, 2024

ABSTRACT

We report a detection of galaxy-QSO cross-correlation w_{GQ} in the Sloan Digital Sky Survey (SDSS) Early Data Release (EDR) over $0.2 - 30$ arc-minute scales. We cross-correlate galaxy samples of different mean depths $r' = 19 - 22$ ($\bar{z}_G = 0.15 - 0.35$) with the main QSO population ($i'_Q < 19.2$) at $\bar{z}_Q \simeq 1.6$. We find positive detection in most cases (except for the faintest QSOs, as expected) with up to 8-sigma significance. The amplitude of the signal on arc-minute scales is about 20% at $\bar{z}_G = 0.15$ decreasing to 10% at $\bar{z}_G = 0.35$. This is a few times larger than currently expected from structure formation Λ CDM models on arc-minute scales, but confirms, at a higher significance, previous measurements by several groups. The shape and redshift evolution of w_{GQ} agrees well with being a lensing signal. When compared to the galaxy-galaxy correlation w_{GG} , this results indicate very strong and steep non-linear amplitude for the underlying matter fluctuations: $\sigma \simeq 400$ on scales of 0.2 Mpc/h, in contradiction with non-linear modeling of Λ CDM fluctuations. We also detect a normalized skewness (galaxy-galaxy-QSO correlation) of $S_3 \simeq 21 \pm 6$ at $\bar{z} \simeq 0.15$ ($S_3 \simeq 14 \pm 4$ at $\bar{z} \simeq 0.35$). All these observational trends can be reconciled with flat Λ universe with $\sigma_8 \simeq 1$, provided the linear spectrum is steeper ($n \simeq 1$) than in the Λ CDM model on small (cluster) scales. In the halo model this means steeper profiles. The galaxy distribution roughly traces this matter variance but with an amplitude that is 100 times smaller: ie galaxies are anti-bias with $b \simeq 0.1$ on these small scales. The bias is shown to increase with scale, which extrapolates well to $b \simeq 1$ at $\simeq 10$ Mpc/h.

Subject headings: galaxies: clustering, large-scale structure of universe, cosmology

1. INTRODUCTION

Weak gravitational lensing by foreground large-scale matter density fluctuations could introduce significant density variations in flux-limited samples of high redshift objects, such as QSOs. This is sometimes called magnification bias or cosmic magnification. In principle, it is possible to separate the intrinsic density fluctuations in QSO samples from the weak lensing magnification signal by cross-correlating the QSOs with a low redshift galaxy sample. This allows a direct measurement of how the galaxy distribution traces the underlying mass distribution. Much work have been done in this direction both on theory and observations (for recent reviews see Norman & Williams 2000, Bartelmann & Schneider 2001, Benítez et al. 2001, Guimarães, van de Bruck and Brandenberger 2001).

Correlation of low redshift galaxies and high-redshift AGNs or QSOs typically find significant excesses of foreground objects around the QSO positions (Tyson 1986; Fugmann 1988,1990; Hammer & Le Fèvre 1990; Hintzen et al. 1991; Drinkwater et al. 1992; Thomas et al. 1995; Bartelmann & Schneider 1993, 1994; Bartsch, Schneider, & Bartelmann 1997; Seitz & Schneider; Benítez et al. 1995; Benítez & Martínez-González 1995, 1997; Benítez, Martínez-González & Martín-Mirónes 1997; Norman & Impey 1999; Norman & Williams 2000). On the other hand, there has also been reports of significant anticorrelation between galaxy groups and faint QSOs (see Croom & Shanks 1999 and references therein). Even though the shape of the galaxy-QSO cross-correlation has not yet been well constrained, these results seem qualitatively in agree-

ment with the magnification bias effect, but the amplitude of the correlation is found to be higher than that expected from gravitational lensing models based on Λ CDM.

What is the origin of this discrepancy? Part of the problem could be due to the lack of well-defined and homogeneous samples. After all we are looking for a small effect, may be as low as 1%, and any systematics in the sample definition is likely to introduce cross-correlations at this level (see §2 below). On the other hand we know little about clustering of dark matter on sub-megaparsec scales. Could the discrepancy be due to real deviations from the Λ CDM paradigm?

Recently, Ménard & Bartelmann (2002) and Ménard, Bartelmann & Mellier (2002) have explored the interest of the SDSS to cross-correlate foreground galaxies with background QSO. The SDSS collaboration made an early data release (EDR) publicly available on June 2001. The EDR includes around a million galaxies and 4000 QSOs distributed within a narrow strip of 2.5 degrees across the equator (see Stoughton et al 2002 for details). As the strip crosses the galactic plane, the data is divided into two separate sets in the North and South Galactic caps. The SDSS collaboration has presented a series of analysis (Zehavi et al. 2002, Blanton et al. 2002, Scranton et al 2002, Connolly et al. 2002, Dodelson et al. 2002, Tegmark et al. 2002, Szalay et al. 2002, Szapudi 2002) of large scale angular clustering on the North Galactic strip, which contains data with the best seeing conditions in the EDR. Gaztañaga (2002a, 2002b) presented a first study of bright ($g' \simeq 20$) SDSS galaxies in both the South and North Galactic EDR strip, centering the analysis on the

comparison of clustering to the APM galaxy Survey (Maddox et al. 1990).

In this paper we will follow closely Ménard, Bartelmann & Mellier (2002, MBM02 from now on) proposal to study the galaxy-QSO cross-correlation signal in the EDR/SDSS. The paper is organized as follows. In section §2 we present the samples used and the galaxy and QSO selection. Section §3 is dedicated to the extinction contamination. Section §4 and §5 presents the main results and its interpretation, while §6 and §7 are dedicated to a discussion and a listing of conclusions.

2. QSO AND GALAXY SAMPLES

The galaxy samples are obtained from the EDR and converted into pixel maps of different resolutions as described in Gaztañaga (2002a,2002b). We select objects from an equatorial SGC (South Galactic Cap) strip 2.5 wide ($-1.25 < DEC < 1.25$ degrees.) and 66 deg. long ($351 < RA < 56$ deg.), which will be called EDR/S, and also from a similar NGC (North Galactic Cap) 2.5 wide and 91 deg. long ($145 < RA < 236$ deg.), which will be called EDR/N. These strips (SDSS numbers 82N/82S and 10N/10S) correspond to some of the first runs of the early commissioning data (runs 94/125 and 752/756) and have variable seeing conditions. Runs 752 and 125 are the worst with regions where the seeing fluctuates above 2". Runs 756 and 94 are better, but still have seeing fluctuations of a few tenths of arc-second within scales of a few degrees. These seeing conditions could introduce large scale gradients because of the corresponding variations in the photometric reduction (eg star-galaxy separation) that could manifest as large scale number density gradients (see Scranton et al 2001 for a detail account of these effects). We will test our results against the possible effects of seeing variations, by using a seeing mask (see §3.1).

Redshift targets in the SDSS are selected in r' for galaxies and i' for QSO. Here we use i' for QSO and both i' and r' for galaxies.¹ The first choice has the interest that both galaxies and QSO come from the same photometric reduction and are therefore subject to similar systematics. Galactic extinction is also smaller in this band. The second choice provides a comparison with previous results on galaxy clustering. To maximize the number of galaxies, and therefore the possibility of lensing, we choose broad magnitude bands. We will focus our results in comparing a nearby sample $r' = 19 - 17.5$ ($\bar{z} \simeq 0.15$) with a distant one $i', r' = 22 - 17.5$ ($\bar{z} \simeq 0.35$). Galaxies selected with $i' < 22$ are almost the same (within few percent) to galaxies in $r' < 22$ as the K-correction cancels out with the color evolution (see Fukugita et al. 1996). Here we take the $i' < 22$ band as our nominal choice to minimize extinction (this will give larger area coverage, see below). As we will show, both galaxy-galaxy and galaxy-QSO cross-correlations turn out to be almost identical in $i' < 22$ and $r' < 22$, the only difference being slightly smaller errors in the $i' < 22$ sample. For the bright sample we stick to $r' < 19$ to provide a more direct comparison with previous results on galaxy-galaxy clustering. Using the redshift distributions in Dodelson et al. (2002), the mean redshift for $17.5 < r' < 19$ (with $\simeq 81000$ galaxies) is $\bar{z} \simeq 0.15$, while

$17.5 < i', r' < 22$ (with $\simeq 425000$ galaxies) have $\bar{z} \simeq 0.35$. We will center our analysis over these two samples, which will be sometimes referred to as $r' < 19$ and $i' < 22$.

The 1st and 3rd slices in Figure 1 shows the EDR/S and EDR/N pixel maps for $i' < 18.5$ and 7 arc-minute resolution. Note the "barrel" shape in the EDR/N. As far as we have been able to find out, this seems an unreported artifact in the EDR redshift sample release which does not seem to include redshifts for secondary targets in this equatorial strip (see Stoughton et al 2002 for details). This is not a problem in our analysis other than we are missing a good fraction of the EDR/N because there are no matching redshifts for the QSOs. The top slice in Figure 2 shows a zoom over the central region of EDR/N.

We recovered the QSO sample from the SDSS/EDR as described in detailed in Schneider et al (2002, see also Stoughton et al 2002). We use point-spread function magnitudes for QSO (which will be quoted with a subindex: i'_Q) and Petrosian magnitudes for galaxies (which will be quoted without any subindex: ie i'), as indicated by above references. We have considered two QSO samples. The one obtained directly from the EDR data archive (ie just with `specobj.specClass = 3`) containing 4275 QSOs, which we call EDR/QSO, and the corrected public QSO sample presented in Schneider et al (2002), which we called SDSS/QSO and contains 3851 QSOs. Almost all SDSS/QSO is contained in EDR/QSO. SDSS/QSO contains a handful of additional known radio QSO that are missing in EDR/QSO. More importantly SDSS/QSO is missing most of the low-redshift AGN ($M_i < -23$) and a small number of narrow-line QSO included EDR/QSO.

Out of the EDR/QSO sample we impose two further cuts: `specobj.zStatus > 2` (to exclude failed or inconsistent redshifts) and `specobj.zConf > 0.7` (to exclude redshifts with confidence less than 70%). In both samples we restrict our analysis to $0.8 < z < 2.5$ where the QSO distribution is compact and homogeneous (the lower cut avoids overlap with the galaxy sample). After these cuts the main difference between EDR/QSO and SDSS/QSO are the few missing radio QSO and a few narrow-band emission QSO's. Over 97% of the QSOs are the same and have the same parameters. Both samples are supposed to be photometrically completed to $16.5 < i'_Q < 19.2$ (Schneider et al 2002).

Number counts and the redshift distribution are shown in Fig.4. Note the sharp break in the QSO number counts at $i'_Q \simeq 19$. The short-dashed line shows a power law with $10^{0.4m}$ (which corresponds to $\alpha = 1$ in Eq.[23]). As lensing magnification should be negative for shallower slopes, we cut the QSO sample to $i'_Q < 18.8$ (which contains 952 QSOs for $0.5 < z < 2.5$) and use the $i'_Q > 18.8$ data (which contains 671 QSOs) for comparison. Thus, unless stated otherwise, QSO are selected with $16.5 < i'_Q < 18.8$, which for brevity will be sometimes referred as $i'_Q < 18.8$.

Right panel in Fig.4 shows how the redshift distribution for $i'_Q < 18.8$ of EDR/QSO (histogram) and SDSS/QSO (dashed line) are almost identical, with a mean redshift of $\bar{z}_{QSO} = 1.67$. The redshift distribution for $i'_Q < 19.2$

¹We will use z', i', r', g', u' for 'raw', uncorrected magnitudes, and z^*, i^*, r^*, g^*, u^* for extinction corrected magnitudes. For example, according to Schlegel et al. (1998) $r' = 18$ corresponds roughly to an average extinction corrected $r^* \simeq 17.9$ for a mean differential extinction $E(B - V) \simeq 0.03$.

is very similar (with just higher surface density). Here we will only present results based on EDR/QSO. We have done all the analysis for SDSS/QSO and find identical results in all cases. We choose to present EDR/QSO because it has been automatically produced (in the same pipeline as the galaxies) and because we are not concerned with the astrophysical nature of the QSO in the sample but rather with having a well defined photometric sample of distant objects.

Figure 1 compares the galaxy pixel maps $i' < 18.5$ with the QSO $i'_Q < 18.8$ distribution in the same portion of the sky (QSOs are the 2nd and 4th slices below the corresponding EDR/N and EDR/S galaxies). Figure 2 shows a zoom over the central region of EDR/N. Note that there is no apparent correlation between QSO and galaxies. As we will see below, most of the signal we are seeking for is hidden below the pixel resolution of this map.

3. CORRECTING FOR GALACTIC EXTINCTION

Absorption by Galactic dust can lead to a positive correlation between galaxies and high- z QSOs (see Norman & Williams 1999). Schlegel et al. (1998) extinction maps have a significant differential extinction $E(B-V) \simeq 0.02 - 0.03$ even at the poles. Thus, the extinction correction has a large impact in the number counts for a fix magnitude range. The change can be roughly accounted for by shifting the mean magnitude ranges by the mean extinction. Despite this, extinction has little impact on clustering, at least for $r' < 21$ (see Scranton et al. 2001 and also Tegmark et al. 1998). This is fortunate because of the uncertainties involved in making the extinction maps and its calibration. Moreover, the Schlegel et al. (1998) extinction map only has a 6'.1 FWHM, which is much larger than the individual galaxies and QSO we are interested on. Many dusty regions have filamentary structure (with a fractal pattern) and large fluctuations in extinction from point to point (ie see Fig.3). One would expect similar fluctuations on smaller (galaxy size) scales, which introduces further uncertainties to individual corrections. As we are looking for a very low signal (of order of 1%) we have to be very careful with small systematic effects, such as extinction.

The net effect of extinction is to produce a magnitude absorption A which translates into a change in the local galaxy surface number density N :

$$\Delta_A \equiv \frac{\Delta N}{N} \simeq \alpha A \quad (1)$$

where α is the slope of the number density counts: $N \simeq 10^{\alpha m}$ as a function of magnitude m . If the absorption A were a constant, this would only change the mean number density in a uniform way. Unfortunately extinction is highly variable and produces density fluctuations in the sky:

$$\delta_A \equiv \Delta_A - \langle \Delta_A \rangle = \alpha (A - \langle A \rangle) \quad (2)$$

We thus see that extinction will introduce spurious number density fluctuations in both the galaxy and the QSO distributions:

$$\bar{\delta}_G = \delta_G + s_G \delta_A \quad (3)$$

$$\bar{\delta}_Q = \delta_Q + s_Q \delta_A \quad (4)$$

where $\bar{\delta}_G$ and $\bar{\delta}_Q$ stand for the total observed fluctuations (as opposed to the intrinsic ones, δ_G and δ_Q) and s_G and s_Q are constant numbers characteristic of each population. From the above analysis we can see that extinction will introduce artificial cross-correlations between the galaxy and QSO populations, even when they are intrinsically uncorrelated.² One can correct for this type of effects by using the absorption maps. We can calculate the cross-correlations:

$$\langle \bar{\delta}_G \delta_A \rangle = s_G \langle \delta_A^2 \rangle \quad (5)$$

$$\langle \bar{\delta}_Q \delta_A \rangle = s_Q \langle \delta_A^2 \rangle \quad (6)$$

$$\langle \bar{\delta}_G \bar{\delta}_Q \rangle = \langle \delta_G \delta_Q \rangle + s_G s_Q \langle \delta_A^2 \rangle \quad (7)$$

where we have assumed that the intrinsic galaxy and QSO positions are uncorrelated with extinction. We thus have:

$$\langle \bar{\delta}_G \bar{\delta}_Q \rangle = \langle \delta_G \delta_Q \rangle + \frac{\langle \bar{\delta}_G \delta_A \rangle \langle \bar{\delta}_Q \delta_A \rangle}{\langle \delta_A^2 \rangle} \quad (8)$$

where $\langle \delta_G \delta_Q \rangle$ is the intrinsic cross-correlation (eg from cosmic magnification). As we can measure all $\langle \bar{\delta}_G \delta_A \rangle$, $\langle \bar{\delta}_Q \delta_A \rangle$ and $\langle \delta_A^2 \rangle$ from the maps, the above expression allow us to correct the galaxy-QSO cross-correlation for extinction. The results for this quantities are shown in the left panel of Fig.5. Note how $\langle \delta_A^2 \rangle$ (shown as closed squares) is quite flat. This is due to the lack of resolution on scales $\theta < 10'$. On larger scales, Schlegel et al. (1998) find that the angular spectrum of their absorption maps fit well $P(k) \propto k^{-2.5}$ at all scale which corresponds to $\langle \delta_A^2 \rangle \propto \theta^{+0.5}$, so that fluctuations grow only slowly with scale.

Fig.5 shows the prediction in Eq.[8] as a continuous line, which is close to 2% for the top case (in all cases we are using $i < 19$ pixel maps for both QSO and galaxies). As can be seen in the figure, when we correct the magnitudes for extinction (top panel) the correction is larger than when we use raw (uncorrected) magnitudes (shown in the middle panel). This is surprising, and basically indicates that we are over-correcting for extinction, which introduces correlated fluctuations in the QSO and galaxy maps.

This is illustrated in the right panel of Fig.5 where we show the galaxy-QSO cross-correlation w_{GQ} for maps with extinction corrected magnitudes $i^* < 19$ (closed squares) with w_{GQ} for maps with raw $i' < 19$ (open squares). The dashed line shows again w_{GQ} with extinction corrected magnitudes after subtracting the correction in Eq.[8] (ie continuous line in the top left panel of Fig.5). The agreement is quite good indicating that there is only marginal contamination of extinction in w_{GQ} when we use raw magnitudes (in agreement with the middle left panel of Fig.5). We will therefore use only raw magnitudes from now on.

These results gives us some confident that we can control this type of contamination in w_{GQ} (and also provides a further test to our cross-correlation codes).

²A similar argument and analysis can be made for other systematics, such as seeing variations.



FIG. 1.— Comparison of equatorial projections maps. The top two slices correspond to galaxy (top) and QSOs in SDSS EDR/S (2.5×60 sqr.deg). The bottom two slices shows galaxies and QSOs in SDSS EDR/N (2.5×90 sqr.deg).

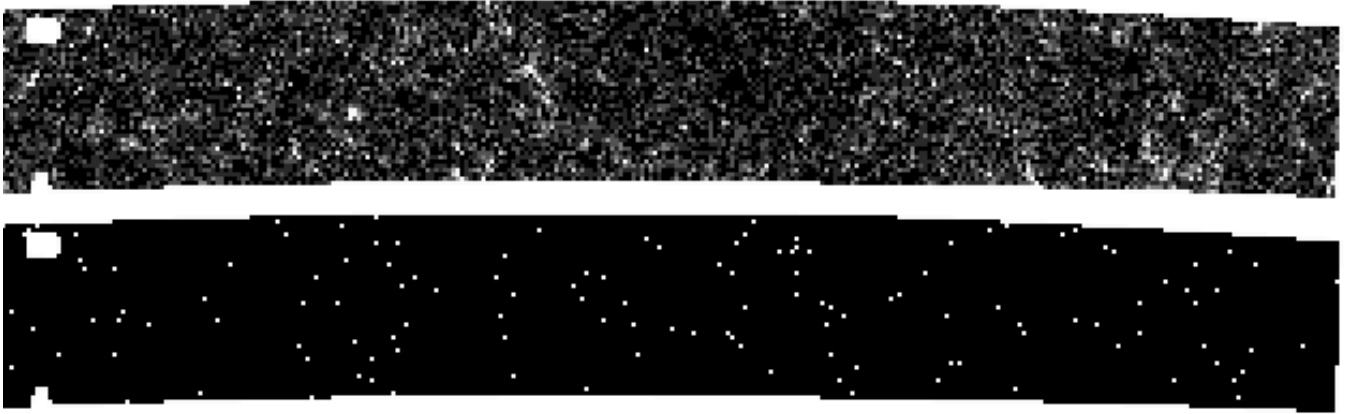


FIG. 2.— Zoom over the central part of the SDSS EDR/N (bottom slices in previous Figure).

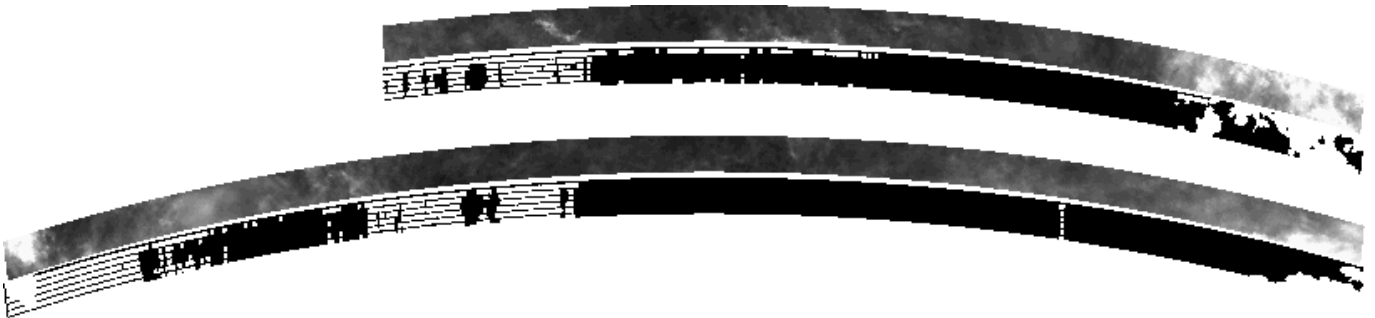


FIG. 3.— Pixel maps of equatorial projections of galactic absorption (from Schlegel et al. 1998) and EDR/SDSS mask of pixels with less than 0.2 mag extinction in i' and less than $2''$ seeing.

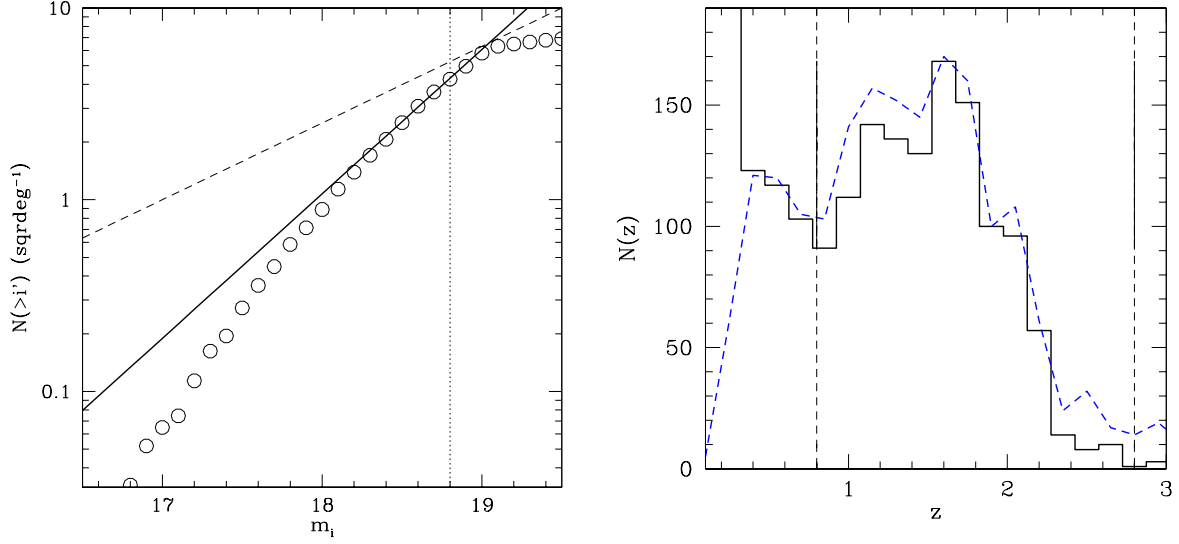


FIG. 4.— LEFT: Integrated QSO number counts per unit magnitude and area. RIGHT: Redshift distributions for the EDR/QSO sample (continuous line) and the SDSS/QSO sample (dashed lines).

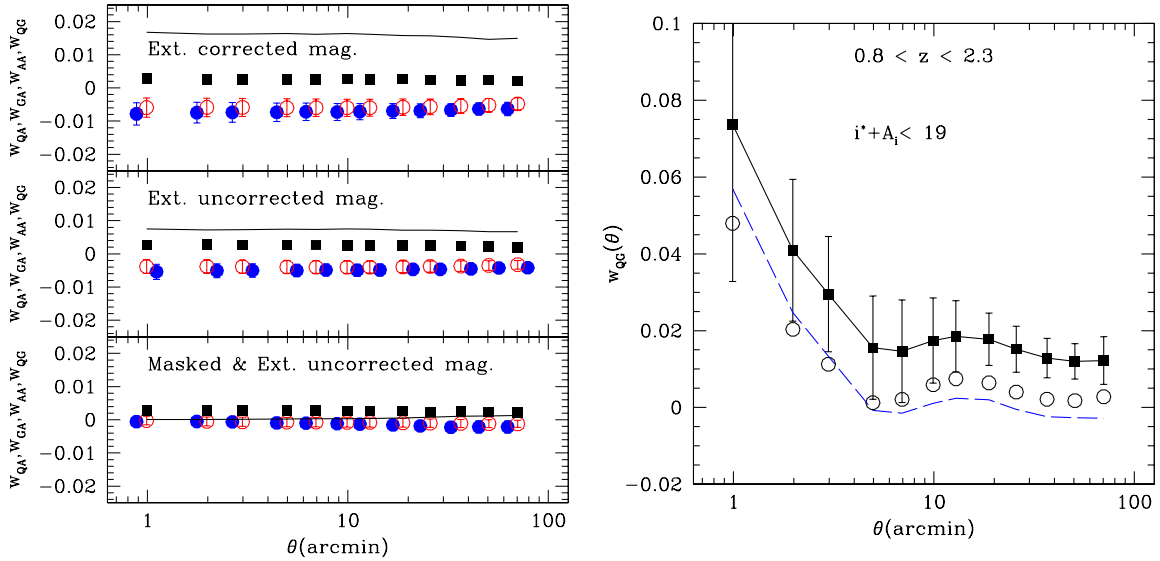


FIG. 5.— LEFT PANEL: The density variance in the extinction $\langle \delta_A^2 \rangle$ (closed squares), compared with galaxy-extinction cross-correlation $\langle \bar{\delta}_G \delta_A \rangle$ (open circles) and the QSO-extinction cross-correlation $\langle \bar{\delta}_Q \delta_A \rangle$ (closed circles). The continuous line shows the contamination in the galaxy-QSO cross-correlation as predicted by Eq.[8]. The top, middle and bottom panel correspond to extinction corrected magnitudes, raw magnitudes and results for raw magnitudes with extinction and seeing mask. RIGHT PANEL: galaxy-QSO cross-correlation w_{QG} as a function of cell radius θ , for objects selected with extinction corrected magnitudes $i^* < 19$ (closed squares and continuous line) and raw magnitudes $i' < 19$ (open circles). The dashed line shows the prediction in Eq.[8] using $\langle \delta_A^2 \rangle$, $\langle \bar{\delta}_G \delta_A \rangle$ and $\langle \bar{\delta}_Q \delta_A \rangle$ cross-correlations shown in the top left panel.

3.1. Extinction and seeing mask

Following Scranton et al (2002), pixels (in 6' resolution) with larger mean seeing or larger mean extinction than some threshold value are masked out from our analysis. The final mask is the product of this seeing and extinction mask (ie shown in Fig.3) by the sample boundary (shown in Fig.2). We have tried different thresholds following the analysis of Scranton et al (2001). As a compromise between precision and area covered, unless stated otherwise, we use 0.2 maximum extinction and seeing better than 1.8' for $r' < 22$ and $i' < 22$. For $r' < 19$ we relax the seeing cut to 2 arc-sec to include more galaxies. For these brighter galaxies 2 arc-sec provides very good photometry for clustering analysis (see Scranton et al. 2001).

Bottom left panel in Fig.5 shows the cross-correlation results after applying the extinction mask over raw $i' < 19$ magnitudes. The resulting contamination in w_{GQ} is negligible.

4. CROSS-CORRELATION MEASUREMENTS

For our statistical analysis, we will use moments of counts in cells, eg the variance:

$$w_{GG}(\theta) = \langle \delta_G^2(\theta) \rangle \quad (9)$$

where $\delta_G \equiv n_G / \langle n \rangle - 1$ are number density fluctuations on cells of size θ (larger than the pixel map resolution) and $\langle n \rangle$ is the mean number of galaxies in the cell. The average $\langle \dots \rangle$ is over angular positions in the sky. We follow closely Gaztañaga (1994, see also Szapudi et al. 1995) and use the same software and estimators here for the SDSS. This software have been tested in different ways and the results confirmed by independent studies (eg see Szapudi & Gaztañaga 1998).

For the cross-correlation we use:

$$w_{GQ}(\theta) = \langle \delta_G(\theta) \delta_Q(\theta) \rangle \quad (10)$$

Note that this is different from the 2-point cross-correlation: $w_2(\theta_{12}) = \langle \delta_G(\theta_1) \delta_Q(\theta_2) \rangle$, where $\theta_{12} = \theta_2 - \theta_1$. In our case, both cells are at the same location in the sky, and the scale dependence comes from changing the cell size. In fact, w_{GQ} is just an area average over w_2 , and its amplitude at scale θ is typically 20 – 30% higher than w_2 at $\theta_{12} \simeq \theta/\sqrt{\pi}$ (see Fig.1 in Gaztañaga 1994). Also note that shot-noise cancels out for cross-correlation w_{GQ} , but not for w_{GG} and w_{QQ} where the variance needs to be shot-noise corrected (eg Gaztañaga 1994).

We will also measure the galaxy-galaxy-QSO 3rd order moment:

$$w_{GGQ}(\theta) = \langle \delta_G(\theta) \delta_G(\theta) \delta_Q(\theta) \rangle \quad (11)$$

and the galaxy-galaxy variance around QSOs:

$$w_{GG;Q}(\theta) = \langle \delta_G(\theta) \delta_G(\theta) \rangle_{QSO} \quad (12)$$

The extra or excess variance is defined as (MBM02):

$$\Delta(\theta) \equiv w_{GG;Q}(\theta) - w_{GG}(\theta) \quad (13)$$

which turns out to be a measure of the 3-point function $w_{GGQ}(\theta) \sim \Delta(\theta)$ (Fry & Peebles 1980, MBM02).

The above statistical quantities have been proposed for galaxy-QSO studies by MBM02. Ménard et al. (2002) also argue that these are the right estimators to improve the accuracy of the comparison with the weak lensing regime.

Errors are obtained from a variation of the jackknife error scheme proposed by Scranton et al (2001, Eq.[10]). These errors has been shown to be reliable when tested against simulations in Zehavi et al (2002) and have the great advantage of being model independent. We also estimate the covariance matrix in this way (Zehavi et al. 2002):

$$Covar(\theta_1, \theta_2) \equiv \langle \Delta w_{GQ}(\theta_1) \Delta w_{GQ}(\theta_2) \rangle \quad (14)$$

In our implementation we use $N = 20$ (but we have also tried $N = 10$ and $N = 40$) independent subsamples of equal size.

4.1. Variance in the galaxy-QSO correlation

The top-left panel of Figure 6 compares the measured values of $w_{GQ}(\theta)$ for the different magnitude bins in $r' = 19, 20, 21, 22$ with $g' = 22$ and $i' = 22$. All cases are roughly consistent with each other. Differences will be studied in section §5, the point here is that there is a significant signal in all bands. Bottom left panel compares $w_{GQ}(\theta)$ when we separate the QSO in high and low redshifts. All cases on the left panels correspond to maps with no extinction mask.

The top-right panel shows in more detail the results for $r' < 19$ ($\bar{z} \simeq 0.15$) and for $i' < 22$ ($\bar{z} \simeq 0.35$). The later have been shifted in angular scale (up by $\simeq 2.2$) to match the $r' < 19$ depth. Closed triangles show the $i' < 22$ results after randomize the angular position of the galaxy counts-in-cells. We expect $w_{GQ} = 0$ in this case, exactly as found within the error-bars. This provides a test for our code and statistics against systematics such as boundary problems in the comparison. Also provides an indication that the errors are not underestimated.

The bottom-right panel in Figure 6 shows the covariance matrix Eq.[14] for $\theta_1 = 0.5$ (continuous line) and $\theta_1 = 1.0$ (dashed line) from the jackknife estimator with $N = 40$ (values for $N = 10$ are comparable but the scatter is larger). As shown in the Figure the dominant contribution comes from the diagonal terms. This is because we are using well separated bins (each cell is 4 times larger than the previous one). We neglect the off-diagonal errors in a first interpretation of the data, but we note that a stronger covariance arises from bins $\theta_2 < \theta_1$ than for $\theta_2 > \theta_1$, as shown in the Figure.

All cases on the right panel of Figure 6 correspond to maps with extinction 0.2 and 2" seeing mask for $r' < 19$ and 1.8" seeing mask for $i' < 22$ (and $i'_Q < 18.8$).

Assuming no covariance, the significance of the detection (against zero correlation) for the first 4 points in top-right panel of Figure 6 is about 4-sigma in $r' < 19$ and 8-sigma in $i' < 22$.

4.2. Faint and Bright QSOs

Bottom left panel in Figure 7 shows a comparison of the results in the EDR/N and EDR/S slices with the combined sample. The agreement is good within the errors, with slightly stronger signal in EDR/S.

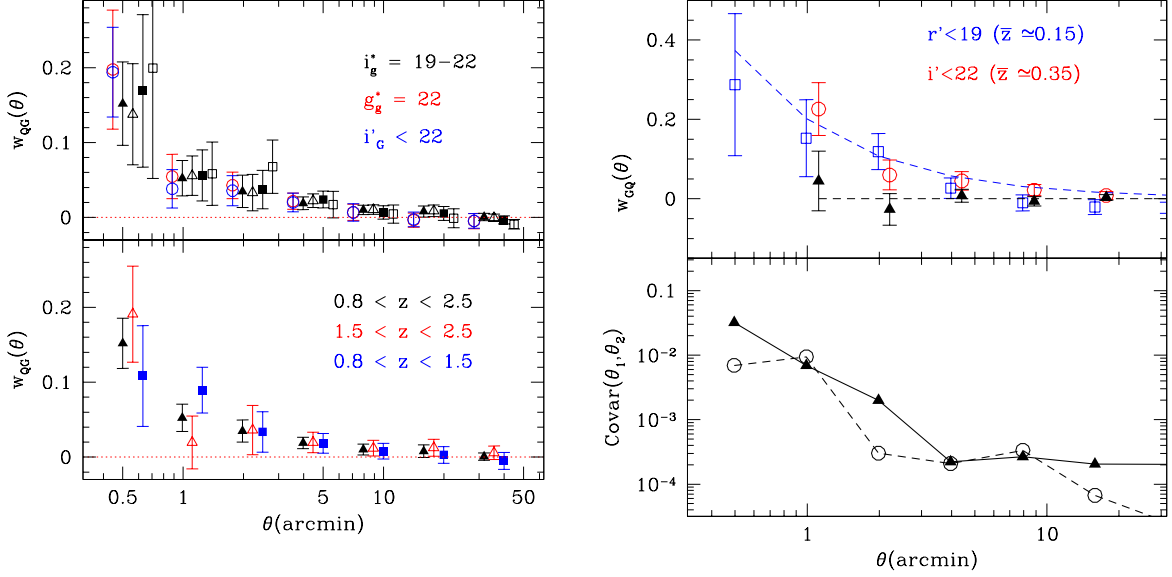


FIG. 6.— TOP LEFT PANEL: QSO-galaxy cross-correlation w_{GQ} (symbols with error-bars) for different galaxy samples. BOTTOM LEFT PANEL: w_{GQ} for $r' = 22$ galaxy sample for different redshift bins in the QSO sample. TOP RIGHT PANEL: Circles and squares with error-bars show galaxy-QSO cross-correlation w_{GQ} for $r' < 19$ ($\bar{z} \approx 0.15$) and for $i' < 22$ ($\bar{z} \approx 0.35$). Closed triangles show w_{GQ} in $i' < 22$ when we randomize the galaxy counts. BOTTOM PANEL: Covariance $\text{Covar}(\theta_1, \theta_2)$ for $\theta_1 = 0.5'$ (continuous line) and $\theta_1 = 1.0'$ (dashed line) as a function of θ_2 .

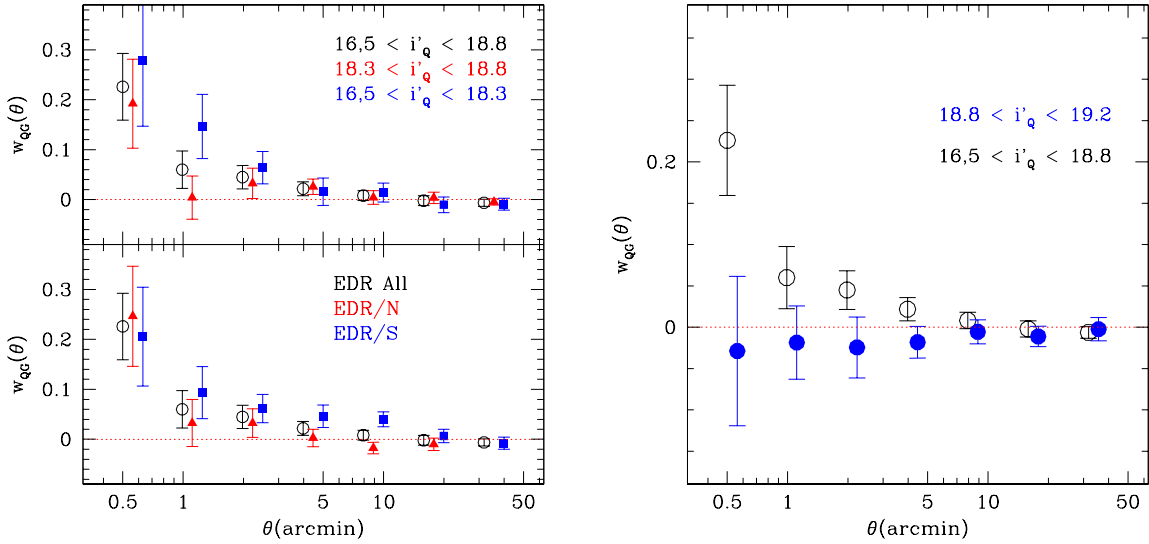


FIG. 7.— TOP LEFT PANEL: galaxy-QSO cross-correlation w_{GQ} for $i' < 22$ galaxies with different QSO sub-samples: $16.5 < i'_Q < 18.3$ (closed squares), $18.3 < i'_Q < 18.8$ (closed triangles) and the combined $16.5 < i'_Q < 18.8$ (open circles). BOTTOM LEFT PANEL: Comparison of the mean w_{GQ} (open circles) with the values in the North (closed squares) and South (closed triangles) EDR subsamples (in all cases $i' < 22$ galaxies and $i'_Q < 18.8$). RIGHT PANEL: Galaxy-QSO cross-correlation w_{GQ} (symbols with error-bars) for $i' < 22$ galaxies with different QSO sub-samples: $16.5 < i'_Q < 18.8$ (open circles) and $18.8 < i'_Q < 19.2$ (closed circles).

Top left panel in Figure 7 shows how the masked $i' < 22$ galaxies cross-correlated with QSO subsamples cut at different $i'_Q < 18.8$ bands. All results agree well within the errors with stronger signal for the brighter QSO, as expected from the steeper slope of the brighter QSOs (see Fig.4).

Left panel in Figure 7 compares w_{GQ} (for masked $i' < 22$ galaxies) for our nominal $16.5 < i'_Q < 18.8$ with the faintest QSOs in EDR/QSO: $18.8 < i'_Q < 19.2$. Note how the fainter QSO sample (closed circles) show no significant cross-correlation. We find a (non-significant) detection of anti-correlation at the 2–3% level. This result is in fact expected (see §5 below) if the cross-correlation is truly due to weak-lensing as $\alpha < 1$ for this faint sample, see Fig.4.

4.3. Comparison to galaxy-galaxy variance

Fig.8 summarizes the main observational results in this paper. We compare $w_{GQ}(\theta)$ (open circles) and $w_{GG}(\theta)$ (closed triangles) for bright $i'_Q < 18.8$ QSOs with faint ($r' < 19$) and bright $i' < 22$ galaxies samples. The dotted line shows (for comparison) the power-law $w_{GQ} = 0.1\theta^{-0.7}$.

All data is well fitted to power-laws taking into account the errors (and neglecting the covariance). We find:

$$\beta_{GG} \equiv \frac{d \log w_{GG}}{d \log(\theta)} = \begin{cases} -0.72 \pm 0.02 & \bar{z} \simeq 0.15 \\ -0.60 \pm 0.03 & \bar{z} \simeq 0.35 \end{cases} \quad (15)$$

$$\beta_{GQ} \equiv \frac{d \log w_{GQ}}{d \log(\theta)} = \begin{cases} -0.83 \pm 0.17 & \bar{z} \simeq 0.15 \\ -0.96 \pm 0.13 & \bar{z} \simeq 0.35 \end{cases} \quad (16)$$

4.4. The Skewness

Fig.9 shows the pseudo-skewness (symbols with error-bars):

$$S'_3(\theta) \equiv \frac{w_{GGQ}(\theta)}{w_{GQ}^2(\theta)} \quad (17)$$

and the normalized excess skewness (continuous lines):

$$S_3^\Delta(\theta) \equiv \frac{\Delta(\theta)}{w_{GQ}^2(\theta)} = \frac{w_{GGQ}(\theta) - w_{GQ}(\theta)}{w_{GQ}^2(\theta)} \quad (18)$$

where w_{GGQ} is the galaxy variance around QSOs. It is expected that both quantities, S'_3 and S_3^Δ , should roughly agree on large scales. In fact, when shot-noise can be neglected $S_3^\Delta = S'_3 - 1$ (see MBM02). Within the errors this relation is in good agreement with Fig.9.

A fit of a constant skewness in Fig.9 gives:

$$S'_3 = \begin{cases} 20.6 \pm 5.7 & \bar{z} \simeq 0.15 \\ 13.6 \pm 4.3 & \bar{z} \simeq 0.35 \end{cases} \quad (19)$$

In Fig.9 we have used the masked mapped with 0.2 red-denning and 2" seeing. Results for other choices of the mask parameters are very similar.

5. COMPARISON WITH PREDICTIONS

5.1. Projection and lens magnification

³At fainter $m_i > 19$ magnitudes the counts show a very sharp break which could be related to possible incompleteness in our sample. Thus, can not estimate the slope reliably for the faint QSO sub-sample $18.8 < i'_Q < 19.2$.

To simplify notation, and without lost of generality, we will give all expression for a flat universe, $\Omega_m + \Omega_\Lambda = 1$, where the comoving angular distance $r(\chi)$ equals the radial comoving distance χ (see Bernardeau, Van Waerbeke & Mellier 1997, Moessner & Jain 1998, for the more general case). Also, by default, assume $\Omega_m = 0.3$, in agreement with current observations (see §6).

The χ distance is given in terms of the redshift z by:

$$d\chi = \frac{dz}{E(z)} \quad ; \quad E(z) = \frac{H_0}{c} \sqrt{1 - \Omega_m + (1+z)^3 \Omega_m} \quad (20)$$

which can be used to map $\chi = \chi(z)$ and $z = z(\chi)$. For $\bar{z} \simeq 0.15$ we find a mean $\chi \simeq 430$ Mpc/h, while $\bar{z} \simeq 0.35$ we have $\chi \simeq 960$ Mpc/h.

The projected galaxy fluctuation is:

$$\delta_G(\theta) = \int_0^{\chi_H} d\chi W_G(\chi) \delta_G(\chi, \theta) \quad (21)$$

where χ_H is the distance to the horizon and θ refers to either the angular position in the sky or the radius of a circular cell in the sky. In the later case, which is the one we will study, δ is smoothed over a cell or radius θ (a cone in the sky). The galaxy selection function $W_G(\chi)$ corresponds to the probability of including a galaxy in the survey and is normalized to unity:

$$\int_0^{\chi_H} d\chi W_G(\chi) = \int_0^z dz n_G(z) = 1 \quad (22)$$

where $n(z)$ is the normalized redshift distribution.

On the other hand, fluctuations in the flux limited QSO induced by weak lensing magnification, δ_μ , can be expressed in terms of the weak lensing convergence \mathcal{K} :

$$\delta_\mu(\theta) = 2(\alpha - 1) \mathcal{K}(\theta) \quad (23)$$

where α is the slope of the QSO number counts:

$$N(> i'_Q) \sim 10^{0.4 \alpha i'_Q} \quad (24)$$

In our sample we find a least square fit of $\alpha \simeq 1.88 \pm 0.03$ in the range $18.4 < i'_Q < 18.9$ (shown as continuous line in Fig.4).³ The convergence is given by a projection over the radial *matter* fluctuation $\delta(\chi, \theta)$, that acts as a lens. This projection is an integral over the lensing magnification efficiency, $\mathcal{E}(\chi)$, a geometrical factor $\simeq \frac{\chi_Q - \chi}{\chi_Q}$ that depends on the QSO χ_Q radial distribution and Ω_m . We express this projection as:

$$\delta_\mu(\theta) = \int_0^{\chi_H} d\chi \mathcal{E}(\chi) \delta(\chi, \theta) \quad (25)$$

where

$$\mathcal{E}(\chi) = 2(\alpha - 1) \frac{3H_0^2 \Omega_m}{2c^2} (1+z) \chi \int_\chi^{\chi_H} d\chi' \frac{\chi' - \chi}{\chi'} W_Q(\chi') \quad (26)$$

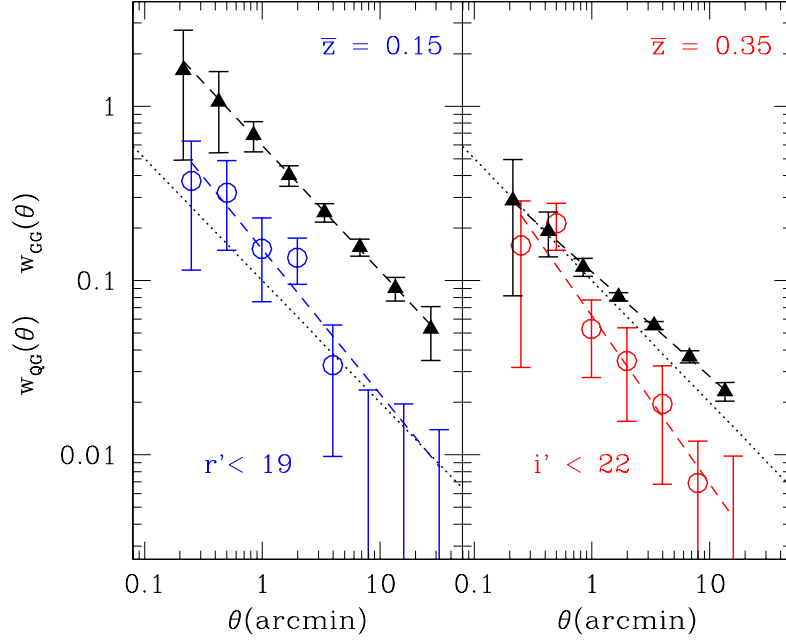


FIG. 8.— Galaxy-galaxy (closed triangles) and galaxy-QSO (open circles) correlation in for bright (left panel) and faint (right panel) galaxies. Dotted-line shows $w_{GQ} = 0.1\theta^{-0.7}$ for comparison, dashed-lines are power-law fits to the data. Galaxy-galaxy correlations have been shifted slightly to the left of the corresponding galaxy-QSO values to avoid intersection of the error-bars.

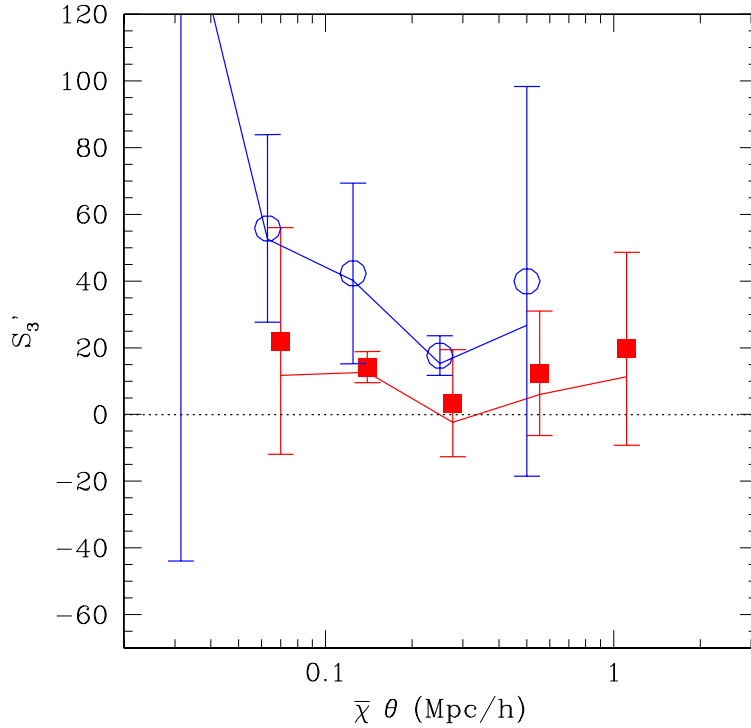


FIG. 9.— Pseudo-Skewness Eq.[17] as a function of θ . Square (circles) correspond to $\bar{z} \simeq 0.35$ ($\bar{z} \simeq 0.15$). Continuous lines in each case correspond to the excess skewness Eq.[18].

and $W_Q(\chi)$ is given by the normalized probability to include a QSO in our sample:

$$\int_0^{\chi_H} d\chi W_Q(\chi) = \int_0^{z_H} dz n_Q(z) = 1 \quad (27)$$

As noted in Bernardeau, Van Waerbeke & Mellier (1997), the crucial difference between galaxy projection in Eq.[21] and lensing magnification in Eq.[25] is that \mathcal{E} is not normalized to unity. Thus, besides the projection effect, which can be modeled as an stochastic selection function, we have an overall re-scaling of fluctuation amplitudes (this has been used in Gaztañaga & Bernardeau 1998 to produce simple non-linear weak-lensing simulations). Figure 10 compares $\mathcal{E}(z)/E(z)$ with $n_G(z)$ and $n_Q(z)$ for the QSO and galaxy samples in our analysis. For QSOs the redshift distribution is the one measured in the EDR/QSO 16.5 < i_Q < 18.8 sample, while for galaxies we show the predictions in Dodelson et al. (2001).

5.2. Mass-mass and galaxy-galaxy correlations

Consider the case of power-law correlations: $\xi(r) = (\frac{r_0}{r})^\gamma$ or $P(k) \sim k^n$, with $\gamma = n + 3$. In current models of structure formation n or γ vary only smoothly with scale, so this should be a good approximation if we limit our study to a small range of scales. We will normalize the amplitude as:

$$\bar{\xi}(R) = \sigma_{0.2}^2 \left(\frac{0.2 \text{Mpc}/h}{R} \right)^\gamma \quad (28)$$

where $\sigma_{0.2}^2$ refers to the *non-linear* amplitude of mass fluctuations on scales of $0.2 \text{Mpc}/h$. In this regime, and within the small angle approximation (eg see §7.2.1 in Bernardeau et al. 2002), the variance of the projected *mass* fluctuations can be expressed as:

$$w_2(\theta) \equiv \langle \delta^2(\theta) \rangle = \sigma_{0.2}^2 A \theta^{1-\gamma} \quad (29)$$

where

$$A = A(\gamma) = B(\gamma) T_\gamma \overline{W_G^2} \quad (30)$$

$$B(\gamma) \equiv \frac{(3-\gamma)(4-\gamma)(6-\gamma)\Gamma(\gamma/2-1/2)\Gamma(1/2)}{5\gamma 2^{3-\gamma} 9 \Gamma(\gamma/2)}$$

T_γ is a geometrical factor of order unity ($T_\gamma \simeq 0.7 - 0.8$) that comes from the area average over the 2-point function:

$$T_\gamma \equiv \frac{4}{\pi(5-\gamma)} \int_0^1 x dx \int_0^{2\pi} d\phi (1+x^2-2x\cos\phi)^{\frac{1-\gamma}{2}}, \quad (31)$$

and $\overline{W_G^2}$ is given by the radial galaxy selection:

$$\overline{W_G^2} \equiv \int_0^{\chi_H} d\chi W_G^2(\chi) \chi^{1-\gamma} D^2(z) \quad (32)$$

where $D(z)$ accounts for the redshift evolution of the correlation function: eg in the linear regime $D(z)$ is the linear growth factor, in the stable clustering regime $D^2(z) = (1+z)^{-3}$.

The galaxy-galaxy variance, assuming Eq.[A4], is:

$$w_{GG}(\theta) \equiv \langle \delta_G^2(\theta) \rangle = b^2 \sigma_{0.2}^2 A_{GG} \theta^{1-\gamma-2\gamma_b} \quad (33)$$

where A_{GG} is the same as A in Eq.[30] for the new slope: $A_{GG} = A(\gamma + 2\gamma_b)$.

5.3. QSO-QSO and galaxy-QSO correlations

We next want to estimate the galaxy-QSO cross-correlation. We express the angular QSO fluctuations as:

$$\delta_Q(\theta) = \delta_Q^I(\theta) + \delta_\mu(\theta) \quad (34)$$

where $\delta_Q^I(\theta)$ stands for the intrinsic fluctuations while $\delta_\mu(\theta)$ are fluctuations induced by magnification bias. Neglecting the QSO (source) and matter (lens) cross-correlation (which is negligible given the large radial separations), the observed QSO variance has two contributions:

$$w_{QQ}(\theta) \equiv \langle \delta_Q(\theta) \delta_Q(\theta) \rangle = w_{QQ}^I(\theta) + w_{\mu\mu}(\theta) \quad (35)$$

where:

$$w_{\mu\mu}(\theta) \equiv \langle \delta_\mu^2(\theta) \rangle = \sigma_{0.2}^2 A_{QQ} \theta^{1-\gamma} \quad (36)$$

with:

$$A_{QQ} = B(\gamma) T_\gamma \overline{\mathcal{E}^2} \quad (37)$$

$$\overline{\mathcal{E}^2} \equiv \int_0^{\chi_H} d\chi \mathcal{E}^2(\chi) \chi^{1-\gamma} D^2(z).$$

The above expressions can be used, for a known magnification, to separate the intrinsic from the apparent QSO clustering.

The QSO and galaxy populations are well separated in radial distances so that we can neglect the intrinsic cross-correlation $\langle \delta_G(\theta) \delta_Q^I(\theta) \rangle$. We then have:

$$w_{GQ}(\theta) \equiv \langle \delta_G(\theta) \delta_Q(\theta) \rangle = \langle \delta_G(\theta) \delta_\mu(\theta) \rangle \quad (38)$$

so that using Eq.[25] and assuming Eq.[A4] we find:

$$w_{GQ}(\theta) = b \sigma_{0.2}^2 A_{GQ} \theta^{1-\gamma-\gamma_b}, \quad (39)$$

with:

$$A_{GQ} = B(\gamma + \gamma_b) T_{\gamma+\gamma_b} \overline{W_G \mathcal{E}} \quad (40)$$

$$\overline{W_G \mathcal{E}} \equiv \int_0^{\chi_H} d\chi W_G(\chi) \mathcal{E}(\chi) \chi^{1-\gamma-\gamma_b} D^2(z)$$

5.4. Measure of bias and matter fluctuations

The combination galaxy-galaxy and galaxy-QSO cross-correlation will allow us to break the intrinsic degeneracy between biasing and matter fluctuations, eg between $b_{0.2}$ and $\sigma_{0.2}$ as measured by galaxy surveys alone. Here, we propose to measure the four parameters that characterize bias and matter fluctuations in a narrow range of scales (the power-law approximation). These parameters are $\sigma_{0.2}^2$ and γ for the variance in non-linear *mass* fluctuations (eg Eq.[28]) and b, γ_b for the bias function as described in the Appendix, eg Eq.[A4].

We can estimate these four parameters, $\sigma_{0.2}, b_{0.2}, \gamma$ and γ_b , from the angular observations of galaxy-QSO correlations in the following way. We first take the measured logarithmic slopes of w_{GG} and w_{GQ} in Eq.[15]-[16] from a

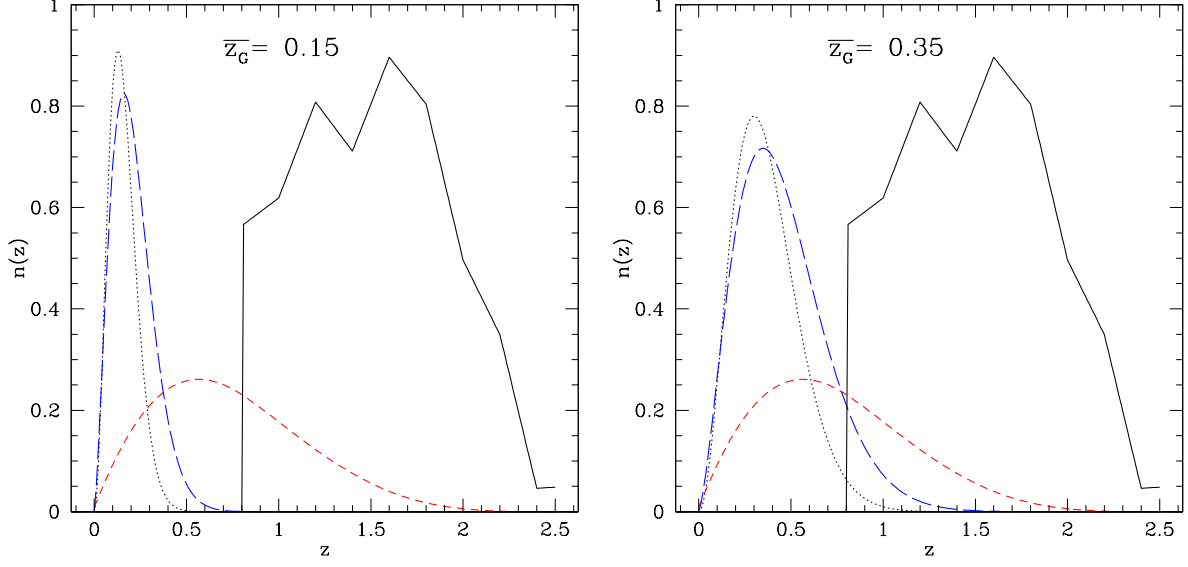


FIG. 10.— The dotted line shows the predicted galaxy redshift distribution $n_G(z)$ (divided by 3 to be on scale) for $z_m = 0.35$ (right panel), which corresponds to $r' < 22$ (and also $i' < 22$) and for $z_m = 0.15$ (left panel), which corresponds to $r' < 19$). The continuous line shows the normalized QSO redshift distribution $n_Q(z)$ as measured in EDR/QSOs. Short-dashed line is the lensing magnification efficiency $\mathcal{E}(z)/E(z)$ for the shown $n_Q(z)$. The long-dashed line corresponds to $\sqrt{n_G(z) \mathcal{E}(z)/E(z)}$ which roughly represents the efficiency of galaxy-QSO cross-correlation.

fit to the data in Fig.8, to find the intrinsic *matter* slope γ and bias scale dependence γ_b :

$$\begin{aligned} \gamma &= 1 + \beta_{GG} - 2\beta_{GQ} \\ \gamma_b &= \beta_{GQ} - \beta_{GG} \end{aligned} \quad (41)$$

We can then obtained $b_{0.2}$ and $\sigma_{0.2}$ as:

$$\begin{aligned} b_{0.2} &= \frac{w_{GG}(\theta)}{w_{GQ}(\theta)} \frac{A_{GQ}}{A_{GG}} \theta^{\gamma_b} \\ \sigma_{0.2}^2 &= \frac{w_{GQ}^2(\theta)}{w_{GG}(\theta)} \frac{A_{GG}}{A_{GQ}^2} \theta^{\gamma-1} \end{aligned} \quad (42)$$

If the power-law model is a good approximation these values should not be a strong function of scale. This will provide a consistency test for our power-law approximation.

The above reconstruction scheme has been tested against mock angular simulations in Gaztañaga (1995). This method can be generalized to extract the shape $\bar{\xi}(R)$ from $w_{GG}(\theta)$ in the quasi-scale invariance approximation by performing local inversions around $R \simeq \theta\chi$, where χ is the mean depth of the sample (see Gaztañaga 1995 for details). We have also verified the validity of such approximations over the weak lensing simulations presented in Gaztañaga & Bernardeau (1998).

5.5. Scale dependence bias

Left panel of Fig.11 shows b/r defined in Eq.[A13] and de-projected from the data at each point as

$$\frac{b}{r} = \frac{w_{GG}}{w_{GQ}} \frac{A_{GQ}}{A_{GG}}, \quad (43)$$

ie assuming that b/r is scale independent (ie $\gamma_b = 0$). Each point is shown at scale corresponding to the mean depth in the sample $\chi\theta$. The resulting values of b/r show a tendency to increase with scale, which means that $\gamma_b = 0$ is not such a good approximation.

Right panel of Fig.11 shows the recovered values of $\sigma_{0.2}$ and $b_{0.2}$ as a function of scale given the prescription in Eq.[42]. The recovered values are quite flat, in good agreement with the power-law assumption.

5.6. Results for $\sigma_{0.2}$, $b_{0.2}$, γ and γ_b

From Eq.[15]-[16] and Eq.[41]:

$$\gamma = \begin{cases} 1.94 \pm 0.34 & \bar{z} \simeq 0.15 \\ 2.33 \pm 0.26 & \bar{z} \simeq 0.35 \end{cases} \quad (44)$$

$$\gamma_b = \begin{cases} -0.11 \pm 0.17 & \bar{z} \simeq 0.15 \\ -0.36 \pm 0.13 & \bar{z} \simeq 0.35 \end{cases} \quad (45)$$

While the mean values from right panel of Fig.11 are:

$$b_{0.2} = \begin{cases} 0.09 \pm 0.02 & \bar{z} \simeq 0.15 \\ 0.09 \pm 0.02 & \bar{z} \simeq 0.35 \end{cases} \quad (46)$$

$$\sigma_{0.2} = \begin{cases} 412 \pm 97 & \bar{z} \simeq 0.15 \\ 364 \pm 86 & \bar{z} \simeq 0.35 \end{cases} \quad (47)$$

These values assume that clustering is fixed in comoving coordinates. Values for other clustering evolution, ie $\epsilon \neq 0$, can be obtained using in Eq.[32]:

$$D^2(z) \simeq (1+z)^{-(3+\epsilon)} \quad (48)$$

If we require the underlaying ($z = 0$) $\sigma_{0.2}$ to be the same in both samples we find:

$$\epsilon \simeq 0.8 \pm 1.3 \quad (49)$$

which roughly agrees with stable clustering, but has a large error.

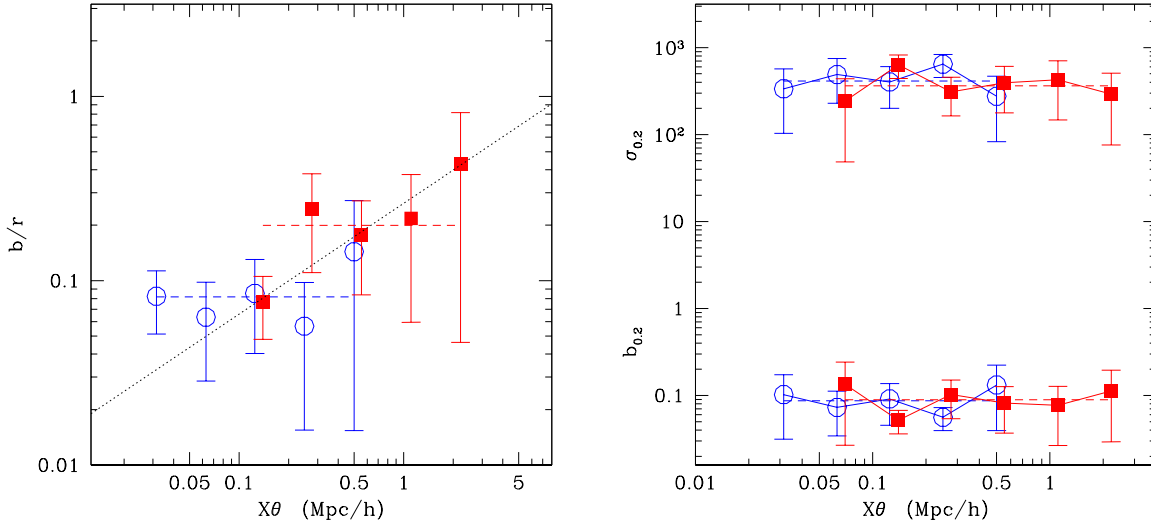


FIG. 11.— LEFT PANEL: Values of b/r de-projected from the ratio w_{GG}/w_{GQ} assuming a constant, but stochastic, bias. RIGHT PANEL: Values of $b_{0.2}$ and $\sigma_{0.2}$ de-projected using Eq.[42], as a function of scale.

6. DISCUSSION

6.1. Unrealistic or correlated error-bars?

We have sliced the data, as displaced in Fig.1, in $N = 10 - 40$ RA bins (horizontal direction in the Figure). Because of the mask, this results in sub-samples with different shapes and holes, which increases the sample-to-sample scatter. Thus we believe that this approach is conservative and slightly overestimates the error-bars. We have tested this idea with the APM (Maddox et al. 1990) pixel maps.

We compare the jackknife error over a given slice out of the APM map against the scatter from different slices (the APM can fit over 20 EDR slices). The jackknife error is comparable to the zone to zone scatter on scales larger than a few arc-minutes (where the mean density of galaxies in a cell is larger than unity), but is about a factor of 3 larger than the zone to zone errors on the smallest scales (dominated by shot-noise fluctuations). We do not attempt to correct for this here, but rather take the conservative approach of using the jackknife errors. This means that in principle the significance of the analysis presented below can be improved with a more sophisticated treatment of errors (eg see Colombi, Szapudi & Szalay 1998).

There is also an overall shift in the mean amplitude due to large scale (sample size) density fluctuations, which is not taken into account by the jackknife error. The amplitude of this effect is comparable to the jackknife error on $20'$ scales. This is similar to an overall calibration error as indeed corresponds to the uncertainty in the value of the mean density over the whole map (eg see Hui & Gaztañaga 1999). Our error analysis hardly changes if we take this into account as we are mostly dominated by the (relatively large) scatter from shot-noise and small scale fluctuations.

Other than this, the covariance shown in bottom-right panel of Figure 6 seems to be dominated by the diagonal terms and we have neglected it.

6.2. Variable obscuration from the Galaxy

Could our result be caused by small scale variations from obscuration in our galaxy? In §3 we have shown that large scale extinction is not affecting our results. There is a small but significant anti-correlation of the SDSS/EDR galaxy and QSO maps with Schlegel et al. (1998) which induces an artificial galaxy-QSO cross-correlation. We have shown how this effect disappears when using an extinction mask. But Schlegel et al. (1998) maps have a FWHM of $\theta = 6'$, while we measure correlations below $\theta = 1'$. Could our cross-correlation be caused by extinction at smaller scales? The spectrum of extinction fluctuations as measured by Schlegel et al. (1998), $P(k) \propto k^{-2.5}$ at scales from $\simeq 6$ arc-min to $\simeq 30$ degrees. , indicates that the amplitude of density fluctuations induced by absorption $\langle \delta_A^2 \rangle \propto \theta^{+0.5}$ grows slowly with scales. Thus extinction produces larger galaxy-QSO artifacts on larger scales.

Extrapolating this spectrum to smaller scales should produce smaller contributions than the ones we have already estimated in §3. In summary, the detected galaxy-QSO cross-correlation have therefore the wrong amplitude and the wrong shape to be explained by galactic extinction.

6.3. The standard Λ CDM picture

In the non-linear regime dark-matter (Λ CDM) numerical simulations typically find that on cluster scales ($r \simeq 0.1$ Mpc/h) the non-linear variance of density fluctuations is $\bar{\xi}_{NL} \simeq 10^2 \bar{\xi}_L$, where $\bar{\xi}_L$ stands for the linear value (compare continuous line with short-dashed line in left panel of Fig.12). Moreover $\bar{\xi}_{NL} \simeq R^{-1}$ ($\simeq R^{-3/2}$ at the non-linear transition) which is typically steeper than the linear values $\bar{\xi}_L \simeq R^{-1/2}$ ($\simeq R^{-1}$ at the non-linear transition). This behavior is reproduced by the non-linear fitting formulae (eg Peacock & Dodds 1996) and have been extensively used in weak-lensing predictions (eg Bartelmann & Schneider 2001, Benitez et al. 2001). For the galaxies, the

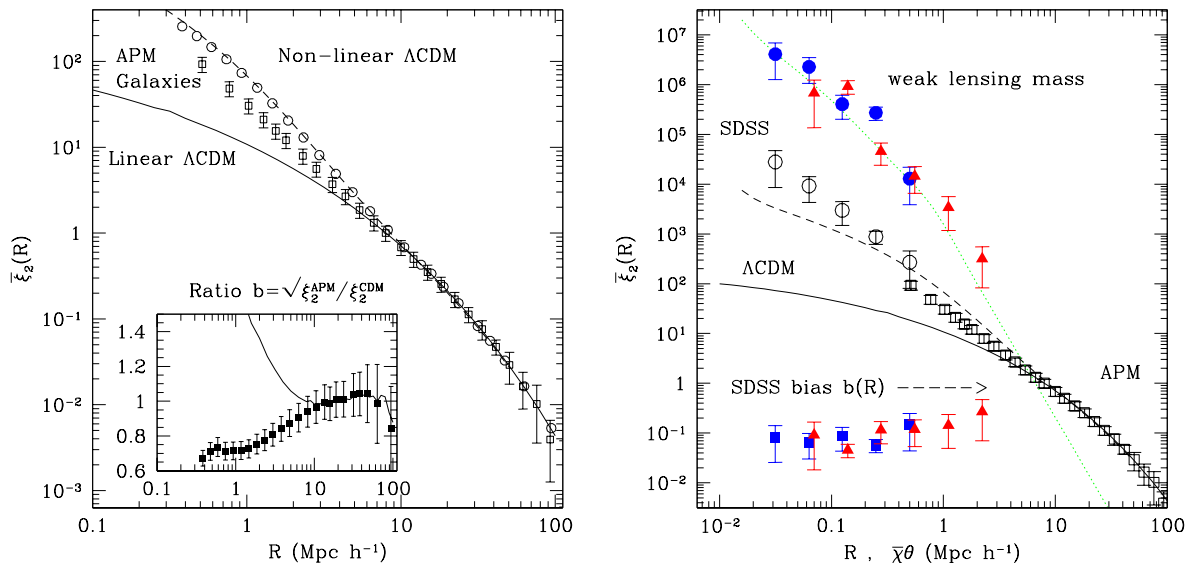


FIG. 12.— LEFT PANEL: Comparison of the linear (continuous line) and non-linear (open squares) variance in the Λ CDM simulations with that in APM galaxies (squares with error-bars), from Fig.11 in Gaztañaga (1995). Dashed lines shows the non-linear fitting formulae of Smith et al. (2002). RIGHT PANEL: Comparison of the linear (continuous line) and non-linear (dashed line) variance in the Λ CDM model with that from the $b_J < 20$ APM galaxies (open squares with error-bars) and $r' < 19$ SDSS galaxies (open circles with error-bars). Upper (lower) closed circles and triangles show the non-linear variance (bias) reconstructed from the galaxy-QSO correlation in the EDR/SDSS at $\bar{z} \simeq 0.15$ and $\bar{z} \simeq 0.35$ (scaled to $z = 0$ under stable clustering). The dotted line shows the non-linear variance for a steep $n_{eff} \simeq 0.97$ initial spectrum.

predictions vary from model to model but one can typically find $\bar{\xi}_G \simeq \bar{\xi}_L$ for blue (Late-type) galaxies and up to $\bar{\xi}_G \simeq 10\bar{\xi}_{NL}$ for the red (Early-type) population. This gives a range $b \simeq \sqrt{\bar{\xi}_G/\bar{\xi}_{NL}} \simeq 0.1$ and $b \simeq 10$. This is also in rough agreement with the estimations in galaxy surveys. We will call this the *standard Λ CDM picture* for non-linear galaxy and mass evolution (see Cooray & Sheth 2002 for an excellent review on all the above ideas).

In terms of the variance most of these features can be summarized in the left panel of Figure 12, which is an expanded version of Fig.11 in Gaztañaga (1995). Note how APM galaxies seem to be anti-bias on small scales with respect to the Λ CDM model, something that seems to be compatible with different models of galaxy formation (eg Jenkins et al. 1998, Seljak 2000, Scoccimarro et al. 2001a, Sheth et al. 2001 and references therein).

6.4. Weak lensing magnification

If we take the detected galaxy-QSO cross-correlation signal as being purely due to weak lensing magnification, we find important challenges for the above picture, even in the orders of magnitude involved. These are summarized in left panel of Fig.12, which shows the recovered mass variance as a function of scale. We find $b \simeq 0.1$ (which seems to agree with the above blue galaxy model above) but with $\bar{\xi}_{NL} \simeq 10^4 \bar{\xi}_L$, so that $\bar{\xi}_G \simeq 10^2 \bar{\xi}_L$ (in agreement with observations and with the standard idea that $b \simeq 1$ when we take $\bar{\xi}_{NL} \simeq 10^2 \bar{\xi}_L$).

We also find some evolutionary trends. First of all, we find $\bar{\xi}_{NL} \simeq R^{-2}$ which is steeper (3 sigma significance) than in the *standard Λ CDM picture*. At higher redshifts ($\bar{z} \sim 0.35$) the slope seems slightly steeper $\bar{\xi}_{NL} \simeq R^{-2.3}$, as expected if we assume that on average there are lower mass halos at higher redshifts, and therefore steeper pro-

files (see Navarro, Frenk & White 1996). Obviously, the slope of the galaxy $\bar{\xi}_G$ distribution is the same as in the *standard Λ CDM picture* (as these are direct observations that we also reproduce in our analysis).

The measured values of the amplitude today $\sigma_{0.2} \simeq 400$ is about 100 times larger than expected in the *standard Λ CDM picture* above (although this depends strongly on the particular cosmology). The significance of this result is over 4-sigma.

The biasing amplitude b at 0.2 Mpc/h remains constant $b \simeq 0.1$ with redshift. The null hypothesis of $b = 1$ is ruled out at a large significance. The slope γ_b seems to become more negative at $\bar{z} \sim 0.35$ (only 1-sigma effect), which partially masks the steepening of the density profiles as we increase the redshift.

On weakly non-linear scales, the shape of the galaxy 3-point function and bispectrum can be used to determine b with independence of the underlying spectrum. This was first proposed by Frieman & Gaztañaga (1994) and Fry (1994), following the ideas in Fry & Gaztañaga (1993). Recent measurements (Frieman & Gaztañaga 1999, Scoccimarro et al. 2001b, Verde et. al 2002) find $b \simeq 1$ at scales > 10 Mpc/h. In fact this value is not in contradiction with the values above as the bias seems to increase with scale, which extrapolates well to $b \simeq 1$ at $\simeq 10$ Mpc/h.

Our recovered values do not assume any model for the primordial spectrum or its subsequent evolution, but assumed a flat geometry with $\Omega_m = 0.3$. This affects both the projection and the amplitude of the lensing magnification. The geometry enters in both the lensing and the galaxy projections and should therefore cancel out to some extent for b , but not quite for $\bar{\xi}_{NL}$ which is estimated from ratio w_{GQ}^2/w_{GG} . Thus we expect our estimations of b to scale with $\simeq \frac{\Omega_m}{0.3}$ and $\bar{\xi}_{NL}$ as $\simeq (\frac{0.3}{\Omega_m})^{1.5}$ (see Bernardeau

et al. 1997). Thus if $\Omega_m \simeq 1$ this would produce $b \simeq 0.3$ and $\sigma_{0.2} \simeq 158$. These values are closer to the *standard Λ CDM picture* above but still uncomfortably far from it. Moreover they represent an inconsistency in the value of Ω_m .

If the *standard Λ CDM picture* fails on these small scales, is there any possible alternative?

6.5. Stable clustering

The amplitude of $\bar{\xi}_{NL}$ at 0.2 Mpc/h follows the stable clustering regime (structures are decoupled from the Hubble expansion): $\bar{\xi} \simeq (1+z)^{-(3+\epsilon)}$, with $\epsilon \simeq 0$, indicating that indeed clustering could be dominated by the halo profile (1h) rather than by the relative distribution of halo pairs (2h term in Eq.[86] of Cooray & Sheth 2002). The fact that the recovered amplitudes at redshifts $\bar{z}_1 \simeq 0.15$ and $\bar{z}_2 \simeq 0.35$ follow:

$$\frac{\bar{\xi}(\bar{z}_1)}{\bar{\xi}(\bar{z}_2)} \simeq \left(\frac{1+\bar{z}_1}{1+\bar{z}_2} \right)^{-3} \simeq 1.6 \quad (50)$$

does not involved any parameter fitting and is non trivial given that the raw observed correlation at different redshifts are quite different (eg see Fig.[8]). In other words, there is no reason to expect any systematic effect to mimic this redshift dependence. Note that both in the linear regime $\bar{\xi}_L \simeq D^2 \bar{\xi}_0$ and in the strongly non-linear regime, this ratio should be independent of the amplitude $\bar{\xi}_0$ of the primordial spectrum. The fact that is good agreement with stable clustering on scales where clusters have collapsed is not surprising. Unfortunately the error we find for ϵ in Eq.[49] is too large to draw more significant conclusions.

There is another aspect to stable clustering, which is related to the scale dependence of the correlations. Peebles (1980) have shown that in the stable clustering for a power-law initial spectrum $\bar{\xi}_L \sim R^{-(n+3)}$ (where n is the index of the linear spectrum $P(k) \sim k^n$), the non-linear slope $\bar{\xi}_{NL} \sim R^{-\gamma}$ is:

$$\gamma = \frac{3(n+3)}{5+n} \quad (51)$$

In the Λ CDM models $n \simeq -1.5$ on non-linear scales so that one would expect $\gamma \simeq 1.3$. Smith et al. find that N-body simulations in fact fall a bit short of this prediction, with $\gamma \simeq 1.0$. For other values of n they find that γ increases with the steepness roughly as predicted by the stable clustering, but the measure γ always fall a bit below the stable clustering prediction in Eq.[51] (see Fig. 9 in Smith et al. 2002). It should be noted that the agreement seems to improve for steep slopes: ie at $n = 0$, Smith et al. (2002) find $\gamma \simeq 1.7$ while Eq.[51] gives $\gamma = 1.8$. Also note that Eq.[51] might be valid for stronger non-linearities (or smaller scales) than tested in the Smith et al (2002) simulations.

Thus, the value we find from the galaxy-QSO data, $\gamma \simeq 2$, indicates a spectrum $n \simeq 1$ in Eq.[51]. This value is very different from the *standard Λ CDM picture*. But we will now show that in fact, for such steep initial spectrum normalized to $\sigma_8 \simeq 1$, one expects the non-linear amplitude to be $\sigma_{0.2} \simeq 400$, just as found in the our interpretation of the galaxy-QSO correlations.

6.6. Non-linearities and halo model

One of the possible origins of the discrepancy that we find with the *standard Λ CDM picture* on small scales is the modeling of the non-linear variance $\bar{\xi}_{NL}$. Based in the stable clustering ideas, Hamilton et al (1991) proposed that the non-linear variance should be a fixed universal function f_{NL} of the linear variance once we identify the adequate mapping of linear to non-linear scales: $\bar{\xi}_{NL} \simeq f_{NL}(\bar{\xi}_L)$. Under stable clustering $\bar{\xi}_{NL} \sim a^3$ while $\bar{\xi}_L \sim a^2$, which implies that $\bar{\xi}_{NL} \simeq \bar{\xi}_L^{3/2}$. These transformations were generalized to the power spectrum and to models with $\Omega \neq 1$ by Peacock & Dodds (1994, 1996) and Jain, Mo & White (1995) to provide phenomenological fitting formulae for non-linear clustering which have since been widely used. The range of validity and the accuracy of these initial ansatzes was limited and, when looked in detail, there appears to be a fundamental problem in getting a universal fit that works for scale dependent models (see Baugh & Gaztañaga 1996, Smith et al. 2002).

A more recent realization of this idea involves the dark matter halo approach (see Cooray & Sheth 2002 for a review) which assumes that the density field can be modeled by a distribution of clumps of matter (the halos) with some density profile. The large-scale clustering of the mass in the linear (and weakly non-linear) regime is given by that of the correlation between halos, which should trace the linear (and weakly non-linear) perturbation theory predictions, while the small-scale clustering of the mass arises from a convolution of the halo density profile with itself. Thus, in this model the results from weak-lensing magnification in right panel of Fig.12 mostly traces the halo profiles.

Smith et al. (2002) present new versions of the universal non-linear fitting formulae f_{NL} that incorporate these new ideas. The new formulae seems to perform quite well against the Virgo N-body simulations. For the Λ CDM model, the comparison involves scales up to $k \simeq 20$ h/Mpc, which corresponds to $R \simeq \pi/k \simeq 0.16$ Mpc/h, comparable to the ones of interest here. We will therefore use this new formulae for f_{NL} (as implemented in the software made publicly available in Smith et al. 2002), to compare to our results. As a first test, left panel of Fig.12 shows the Smith et al. (2002) non-linear prediction (dashed-line) against our N-body results from Λ CDM simulation (opened circles). The agreement is excellent and does not involve any additional parameter fitting. It should be noted that the differences with previous fitting formulae (eg Peacock & Dodds 1996) in this particular case are small. This is important as it means that Λ CDM predictions for galaxy-QSO cross-correlations on non-linear scales in the literature are correct and we need to look elsewhere for the origin of the discrepancy.

As can be seen in the right panel of Fig.12 the weak-lensing magnification predictions show a very steep non-linear variance, $\gamma \simeq 2$, which in the context of stable model or direct simulation (see §6.5 above) can be interpreted as indication of a steep linear spectrum $n_{eff} \simeq 0.9 - 1.0$. This steep linear spectrum can be obtained from the Smith et al. (2002) formulae by using a large effective value of the shape parameter Γ . For example, $\Gamma = 200$ ($\sigma_8 = 1$, $\Omega_m = 0.3$ and $\Omega_\Lambda = 0.7$) produces $n_{eff} = 0.96$. This

prediction is shown as a dotted-line in left panel of Fig.12. This illustrates the point that we need a large positive slope to fit the data. Note that, once we fix the slope (from the same measurements) the only free parameter is σ_8 , which we take to be $\sigma_8 = 1$ for consistency with power spectrum measurements (eg Tegmark & Zaldarriaga 2002 and references therein) and with the higher order correlations (see Bernardeau et al. 2002 and references therein).

This means that in fact, that shape and amplitude for $\bar{\xi}_{NL}$ that we find from weak-lensing are compatible with the general picture of non-linear evolution of clustering and with the $\sigma_8 = 1$ normalization. Under this assumption the only difference with the *standard Λ CDM picture* is that the linear spectrum on small (non-linear) scales has to be steeper. If we match this with the *standard Λ CDM $P(k)$* on larger scales, this requires $P(k)$ to turn around and increase (rather than decrease) on galactic scales. As these scales are not strongly constraint by other observations (see below), the contradiction can be resolved in this way.

6.7. Ω_m dependence and Skewness

Other alternatives to the above considerations on non-linear modeling are to change the value of Ω_m and Ω_Λ but keeping $n_{eff} \simeq -1.5$ (eg with a low shape parameter).

Open models with $\Omega_m \simeq 0.01$ have more power on small scales, just as we need to explain the data. This does not seem to work for two reasons. First, because if we lower Ω_m the weak lensing magnification signal becomes smaller which translates into a higher value of the recovered mass $\bar{\xi}_{NL}$. Second, because the non-linear slope γ is too low compare to the weak-lensing reconstruction.

As mentioned above (end of §6.4) closed models with $\Omega_m \simeq 1$ predict a three times stronger weak lensing magnification signal. This translates into a nine times smaller reconstructed variance and three times larger biasing, which is still not able to reconcile the discrepancy with the standard predictions for the amplitude of non-linear matter fluctuations.

Bernardeau et al (1997) predicted $S_3 \simeq -40\Omega_m^{-0.8}\bar{z}_{QSO}^{-1.35}$ for the convergence skewness S_3 in the Λ CDM model. One should roughly expect $S'_3 \simeq -S_3$, so that a direct comparison with Eq.[19] using our mean $\bar{z}_{QSO} = 1.67$ yields $\Omega_m \simeq 1.08^{+0.31}_{-0.65}$. This is high and about 3 sigma out of the currently favored value of $\Omega_m \simeq 0.3$ (eg Tegmark & Zaldarriaga 2002 and references therein). Note nevertheless that is just a very rough comparison, both because we need to take into account non-linear effects (see Hui 1999) and because of the differences with pseudo-skewness. A direct comparison can be made to Fig.3 in Ménard, Bartelmann & Mellier (2002), which corresponds to $z_Q \simeq 1.5$. Again here, the values for S'_3 in Eq.[19] favor the $\Omega_m \simeq 1$ and seem about 3-sigma away from the $\Omega_m \simeq 0.3$ value. The S_3 predictions are insensitive to the linear (scale dependence) bias and the amplitude and shape of the linear mass spectrum. But note that they are quite sensitive to linear spectrum n_{eff} of fluctuations on non-linear scales as they rely on the so-called saturation value in hyper-extended perturbation theory (Scoccimarro & Frieman 1999). If we change the value from $n_{eff} \simeq -1.5$ to $n_{eff} \simeq 0.9$, as suggested by the non-linear slope γ (see §6.5 above) then we get a value for S_3 which is about 5 times smaller. We thus have

$S_3 \simeq 8\Omega_m^{-0.8}\bar{z}_{QSO}^{-1.35}$ which now yields:

$$\Omega_m \simeq 0.15^{+0.05}_{-0.08} \quad (52)$$

in better agreement with the Λ CDM cosmology.

6.8. Comparison with other results

Are our results in contradiction with other measurements of the mass or of the bias? On these scales we have measurements of the spectrum from Ly-alpha forest (Croft et al. 2002), but they are mostly sensitive to the linear regime, as they correspond to higher redshifts. Weak lensing results (Hoekstra et al. 2002) seem to agree well with the *standard Λ CDM picture* above, and therefore seems at odds with the results presented here. In particular, compare $b/r \simeq 1$ in Fig.6 in Hoekstra et al. 2002 with our $b/r \simeq 0.1$ in Fig.11, which are both obtained under the same definitions of biasing parameters. Note nevertheless that our analysis is proving slightly smaller scales, and more importantly note that we do not assume any specific model for the underlying matter fluctuations. If the value of ξ_{NL} is indeed as large as indicated by our analysis one would also expect a stronger aperture mass variance, but given the number of parameters involved in the comparison of data with theory, some other interpretations may still be possible (eg Croft & Metzler 2000, Mackey, White & Kamionkowski 2002). More work is needed to understand this apparent discrepancy. The values of S_3 found by Bernardeau, Van Waerbeke & Mellier (2002) from the VIRMOS-Desart data should also be compared with the pseudo-skewness we find in Fig.9.

7. CONCLUSION

Our results for a strong galaxy-QSO cross-correlation passed several test presented in §3 and §4 and Fig.6-7. In particular note right panel in Figure 7 which shows how the signal disappears for faint QSOs, as expected if produced by weak lensing magnification. Also note in top-left panel of Fig.7 that the brighter the QSO sample the larger the amplitude of the positive detection. The amplitude of the negative cross-correlation signal (of only few percent) is smaller than the positive cross-correlation. This can be understood as $|\alpha - 1|$ in Eq.[24] is smaller for the fainter than for brighter QSOs. Strong galaxy-QSO or cluster-QSO lensing magnification can also contribute to the positive cross-correlation, but one would expect this effect to be stronger for the fainter QSOs (as the mean density is larger and the redshift distribution is very similar). Non-linear corrections to the weak-lensing approximation are typically small for the variance (see Ménard et al. 2002). Thus, weak lensing seems the most plausible lensing explanation for the detected galaxy-QSO correlation.

Fig. 8 and Fig.12 summarized the main results presented in this paper, which seem at odds with the standard Λ CDM model, both because the large amplitude and the steep slope of the recovered variance on non-linear scales. Note that this broad interpretation is independent of the details in our modeling to recover the variance. As can be seen in Fig. 8 we find $w_{GQ} \simeq w_{GG}$ on the smallest scale for $\bar{z} = 0.35$. This alone, indicates that the bias factor b has to be quite small, $b \ll 1$, as weak lensing is typically less efficient than unity. In §6 we argue that a

possible explanation for this strong correlation is that the effective linear spectral slope on small scales is $n_{eff} \simeq 1$, in agreement with Eq.[51]. This is much steeper than in Λ CDM. Within currently accepted cosmological parameters ($\sigma_8 \simeq 1$, $\Omega_m \simeq 0.3$ and $\Omega_\Lambda \simeq 0.7$) adopting $n_{eff} \simeq 1$ can explain at the same time the shape and slope of the recovered variance in Fig.12 and the low skewness in Fig.9.

This is a preliminary analysis from a small fraction of the SDSS early commissioning data. To explain the detected excess galaxy-QSO correlation of $\sim 10\%$ with correlated photometric errors, such as flat-fielding or scatter light, we would need very significant photometric variations: RMS of at least $\Delta i' \simeq 0.3$ on arc-minute scales⁴, which is larger than the nominal calibration uncertainties of 0.03 magnitudes (see Stoughton et al 2002). It is improbable that such large photometric errors are present in the EDR/SDSS as they would have already been detected as an excess galaxy-galaxy correlation when compared to other surveys (eg see Gaztañaga 2002a, 2002b, Connolly et al. 2002, Scranton et al. 2002). Nevertheless, the full SDSS catalog should be able to do a much better analysis of systematics than the one presented here and confirm or refute our findings with a high significance. A larger piece of the SDSS would allow a comparisons to

larger scales, which is missing in our analysis because of the narrow width of the EDR strips. On larger scales, the weak-lensing magnification signal can be more directly compared to other indications of mass clustering, which will be an essential test for cosmology and for the weak lensing magnification nature of these cross-correlations.

ACKNOWLEDGMENTS

I would like to thank R.Scranton and Josh Frieman for useful discussions and comments on the SDSS/EDR data. I also like to thank David Hughes and Marc Manera for stimulating discussions of this work. I acknowledge support from supercomputing center at CEPBA and CIESCA/C4, where part of these calculations were done. I also acknowledge support from and by grants from IEEC/CSIC and the Spanish Ministerio de Ciencia y Tecnología, project AYA2002-00850 and EC FEDER funding.

Funding for the creation and distribution of the SDSS Archive has been provided by the Alfred P. Sloan Foundation, the Participating Institutions, the National Aeronautics and Space Administration, the National Science Foundation, the U.S. Department of Energy, the Japanese Monbukagakusho, and the Max Planck Society. The SDSS Web site is <http://www.sdss.org/>.

REFERENCES

- Bartelmann, M. & Schneider, P. 1993b, A&A, 271, 421
 Bartelmann, M., & Schneider, P. 1994, A&A, 284, 1
 Bartelmann, M., Schneider, P., Phys. Rep., 2001, 340, 291
 Bartsch, A., Schneider, P. & Bartelmann, M., 1997, A&A, 319, 375
 Baugh, C.M., Cole, S., Frenk, C.S., 1996, MNRAS 283, 1361
 Baugh, C.M., Gaztañaga, E., 1996, MNRAS 280 L37
 Benítez, N., & Martínez-González, 1995, ApJL 339, 53
 Benítez, N., & Martínez-González, 1997, ApJ, 477, 27
 Benítez, N., Martínez-González, E., González-Serrano, J.I., & Cayón L. 1995, AJ, 109, 935
 Benítez, N., Martínez-González, E. & Martín-Mirones, J. M. 1997, A&A, 321, L1
 Benítez, N., Sanz, J.L., Martínez-González, E., 2001, MNRAS 320, 241
 Bernardeau, F., Van Waerbeke, Mellier, Y. 1997, A&A 322, 1
 Bernardeau, F., Van Waerbeke, Mellier, Y. 2002, A&A 389, L28
 Bernardeau, F., Colombi, S., Gaztañaga, E., Scoccimarro, R., 2002, Phys. Rep., 367, 1
 Blanton, and the SDSS collaboration, 2002 2001, A.J., 121, 2358
 Colombi, S., Szapudi, I., Szalay, A.S., 1998, MNRAS296, 253
 Connolly and the SDSS collaboration, 2002 astro-ph/0107417
 Cooray, A., Sheth, R., Phys. Rep, in press, astro-ph/0206508
 Croft, R.A.C. et al. 2002, ApJ in press, astro-ph/0012324
 Croft, R.A.C. & Metzler, C.A., 2000, ApJ 545, 561
 Croom, S.M., Shanks, T., 1999, MNRAS307, L17
 Dekel, A., Lahav, O., 1999, ApJ 520, 24
 Dodelson, S., and the SDSS collaboration, 2002 ApJ 572, 140
 Drinkwater, M. J., Webster, R. L., Thomas, P. A. & Millar, E. 1992, Proceedings of the Astronomical Society of Australia, 10, 8
 Frieman, J.A., Gaztañaga, E., 1994, ApJ425, 392
 Frieman, J.A., Gaztañaga, E., 1999, ApJ521, L83
 Fry, J. N. 1994, PRL 73, 215
 Fry, J. N. & Peebles, P.J.E., 1980, ApJ, 238, 785
 Fry, J. N. & Gaztañaga, E. 1993, ApJ, 413, 447
 Fugmann, W. 1988, A&A, 204, 73
 Fukugita, M., et al. 1996, AJ 111, 1748
 Gaztañaga, E., 1994, MNRAS268, 913
 Gaztañaga, E., 1995, ApJ, 454, 561
 Gaztañaga, E., 2002a, MNRAS333, L21
 Gaztañaga, E., 2002b, ApJ 580 in press (astro-ph/0110126)
 Gaztañaga, E., & Bernardeau, F 1998, A&A 331, 829
 Guimarães, A.C.C., van de Bruck, C. Brandenberger, R., 2001, MNRAS, 325, 278
 Hamilton, A.J.S., Kumar, P., Lu, E., Matthews, A., 1991, ApJ Lett., 374, L1
 Hammer, F. & Le Fevre, O. 1990, ApJ, 357, 38
 Hintzen, P., Romanishin, W., & Valdés, F., 1991, ApJ, 371, 49
 Hoekstra, H., Van Waerbeke, L., Gladders, M.D., Mellier, Y., Yee, H.K.C., 2002, Ap.J in press, astro-ph/0206103
 Hui, L. & Gaztañaga, E., 1999, ApJ, 519, 622
 Hui, L., 1999, ApJL, 519, L9
 Jenkins, A., et al. 1998, ApJ, 499, 20
 Jain, B., Mo, H.J., White, S.D.M., 1995, MNRAS 276, L25
 Mackey, J., White, M., Kamionkowski M, 2002, astro-ph/0106364
 Maddox, S.J., Efstathiou, G., Sutherland, W.J. & Loveday, J., 1990, MNRAS, 242, 43P
 Matsubara, T., 1999, ApJ 525, 543
 Ménard, B., Bartelmann, M., Mellier, Y., 2002, A&A submitted, astro-ph/0208361
 Ménard, B., Bartelmann, M. 2002, A&A submitted astro-ph/0203163
 Ménard, B., Hamana, T., Bartelmann, M., Yoshida, N, 2002, A&A submitted, astro-ph/0210112
 Moessner, R. Jain, B. 1998, MNRAS294, 291
 Navarro, J., Frenk, C., White, S.D.M, 1996, ApJ, 462, 563
 Norman, D. J. & Impey, C. D. 1999, AJ, 118, 613
 Norman, D.J. & Williams, L.L.R. 2000, ApJ 119, 2060
 Peacock, J.A., & Dodds S.J., 1994, MNRAS 267, 1020
 Peacock, J.A., & Dodds S.J., 1996, MNRAS 280 L19
 Pen, U-L, 1998, ApJ 504, 601
 Peebles, P.J.E., 1980, The Large-Scale Structure of the Universe, Princeton University Press, Princeton (LSS)
 Schneider, D.P. and the SDSS collaboration 2002, AJ 123, 567
 Scoccimarro, R., Sheth, R.K., Hui, L., Jain, B. 2001a, ApJ, 546, 20
 Scoccimarro, R., Feldman, H., Fry, J. N. & Frieman, J.A., 2001b, ApJ, 546, 652
 Scoccimarro, R., Frieman, J.A., 1999, ApJ 520, 35, 44
 Scranton, R., and the SDSS collaboration astro-ph/0107416, submitted to ApJ.
 Scherrer, R.J., Weinberg, D.H., 1998, ApJ 504, 607
 Seljak, U. ; 2000, MNRAS, 318, 203
 Seitz, S. & Schneider, P. 1995, A&A, 302, 9
 Sheth, R., Diaderio, A., Hui, L. Scoccimarro, R., 2001, MNRAS, 326, 463
 Smith, R.E., et al. 2002, astro-ph/0207664
 Stoughton C. and the SDSS collaboration, 2002 AJ 123, 485
 Szapudi, I. & Gaztañaga, E., 1998, MNRAS300, 493
 Szapudi, I., Dalton, G.B. , Efstathiou, G., Szalay, A.S. 1995, ApJ 444, 520
 Szapudi, I., and the SDSS collaboration, 2002 ApJ 570, 75
 Tegmark, M., Hamilton, A.J.S., Strauss, M.A., Vogeley, M.S. & Szalay, A.S. 1998, ApJ, 499, 555
 Tegmark, M., Zaldarriaga, M., 2002, astro-ph/0207047
 Tegmark, M., and the SDSS collaboration, 2002 ApJ 571, 191

⁴This assumes unity slopes for the number counts $N(m > i')$, realistic slopes require even larger photometric errors.

Tegmark, M., Peebles, P.J.E., 1998 ApJL 500, 79
 Thomas, P.A., Webster, R.L., & Drinkwater, M.J. 1994, MNRAS, 273, 1069

Tyson, J.A., 1986, AJ, 92, 691
 Verde, L., et al. 2002, MNRAS in press
 Zehavi, I., and the SDSS collaboration, 2002 ApJ 571, 172

APPENDIX

GALAXY BIASING

We will consider two different mathematical approaches to parameterize the effects of biasing, ie. how galaxy fluctuations δ_G trace the underlying mass distribution δ . More elaborated physical models are based on semi-analytical galaxy formation (see eg Baugh, Cole & Frenk 1996, Seljak 2000, Scoccimarro et al. 2001, Sheth et al. 2001, Cooray & Sheth 2002) but the results are quite model dependent.

The first model consists in assuming that bias is linear, but non-local:

$$\delta_G(x) = \int d^3x' b(x-x') \delta(x') \quad (\text{A1})$$

Which in Fourier space is just:

$$\delta_G(k) = b(k) \delta(k) \quad (\text{A2})$$

This translates into a scale-dependence bias on the power-spectrum:

$$P_G(k) = b^2(k) P(k) \quad (\text{A3})$$

For a power-law correlation $P(k)$ and a power-law $b(k)$ we have that the galaxy variance is

$$\bar{\xi}_G(R) = b_{0.2}^2 \sigma_{0.2}^2 \left(\frac{0.2 \text{ Mpc}/h}{R} \right)^{\gamma+2\gamma_b} \quad (\text{A4})$$

where b and γ_b characterize the amplitude and scale dependence of the effective bias:

$$b(R) = b_{0.2} \left(\frac{0.2}{R} \right)^{\gamma_b}. \quad (\text{A5})$$

If $\gamma_b = 0$ this reduces to the standard linear biasing model $\bar{\xi}_G(R) = b^2 \bar{\xi}(R)$.

In the second model we assume that bias is non-linear, but local:

$$\delta_G(r) = F[\delta(r)]. \quad (\text{A6})$$

For small fluctuations $\delta < 1$:

$$\delta_G \simeq b_1 \delta + \frac{b_2}{2!} \delta^2 + \frac{b_3}{3!} \delta^3 + \mathcal{O}[\delta^4] \quad (\text{A7})$$

which gives rise to (see Fry & Gaztañaga 1993):

$$\bar{\xi}_G = b_1^2 \bar{\xi} + c \bar{\xi}^2 + d \bar{\xi}^3 + \dots \quad (\text{A8})$$

where $c = (S_3 b_2 b_1 + b_3 b_1 + 0.5 b_2^2)$ depends both on the non-linear biasing parameters and S_3 , the reduced skewness of the mass. Thus, the local model formally gives

$$\bar{\xi}_G = \mathcal{F}[\bar{\xi}] \quad (\text{A9})$$

which reduces to the standard linear biasing model $\xi_G(r) = b^2 \xi(r)$ for $\bar{\xi} \rightarrow 0$. On non-linear scales we can write:

$$\bar{\xi}_G \simeq K \bar{\xi}^\phi, \quad \phi \equiv \frac{d \log \mathcal{F}}{d \log \bar{\xi}} \quad (\text{A10})$$

which reproduces Eq.[A4] with $\phi = 2\gamma_b$ and $K = b_{0.2}^2 / \sigma_{0.2}^{2(1+\gamma_b)}$.

Thus we have shown that two quite different hypothesis about biasing drives to a similar expression, ie Eq.[A4], at least in the power-law limit. It is therefore plausible to assume that a more generic non-local and non-linear biasing could also be cast with such a parameterization. We therefore adopt Eq.[A4] on the assumption that a power-law should be a good approximation for the limited range of scales we consider here. We will be able to somehow test this assumption with the data.

Stochastic bias

The stochasticity of the galaxy-mass relation can also contribute to the observed galaxy clustering (see Pen 1998, Scherrer & Weinberg 1998, Tegmark & Peebles 1998, Dekel & Lahav 1999, Matsubara 1999, Bernardeau et al. 2002, and references therein), so that the relation between δ_G and δ is not deterministic but rather stochastic,

$$\delta_G(r) = F[\delta(r)] + \epsilon_\delta(r) \quad (\text{A11})$$

where the random field ϵ_δ denotes the scatter in the biasing relation at a given δ due to the fact that $\delta(r)$ does not completely determine $\delta_G(r)$. Under the assumption that the scatter is local, in the sense that the correlation functions of $\epsilon_\delta(r)$ vanish sufficiently fast at large separations (i.e. faster than the correlations in the density field), the deterministic bias results hold for the two-point correlation function in the large-scale limit (Scherrer & Weinberg 1998).

This stochasticity is usually characterized by a parameter r defined as:

$$r \equiv \frac{\langle \delta \delta_G \rangle}{b \langle \delta \delta \rangle} \quad \text{with} \quad b^2 \equiv \frac{\langle \delta_G \delta_G \rangle}{\langle \delta \delta \rangle} \quad (\text{A12})$$

which implies:

$$\frac{r}{b} \equiv \frac{\langle \delta \delta_G \rangle}{\langle \delta \delta \rangle} \quad (\text{A13})$$

Note that r and b are mean quantities and both contain information on the scale independence and the stochastic ϵ . This provides a different parameterization of biasing than the one given in the above subsection and has been used by Hoekstra et al. (2002) to characterize the comparison of the weak-lensing and galaxy correlations. To provide a comparison we also present in Fig.11 results for b/r defined in such a way, but note that the meaning of b here is quite different from the one in Eq.[A2] (see Dekel & Lahav 1999).

Note that even though the above has become a standard to parameterize stochastic effects, the parameterization presented above in terms of $b_{0.2}$ and γ_b , is not necessarily in contradiction with the idea that the stochasticity could play an important role in biasing.